Calibration Architecture for the Nonlinear Wheel Odometry Model with Integrated Noise Compensation

Máté Fazekas^{1,2} and Péter Gáspár¹ b

¹HUN-REN Institute for Computer Science and Control, Hungarian Research Network (HUN-REN SZTAKI),

Kende Street 13-17, Budapest, 1111, Hungary

²Department of Control for Transportation and Vehicle Systems, Budapest University of Technology and Economics (BME-KJIT), Stoczek street 2, Budapest, 1111, Hungary

Keywords: Parameter Identification, Wheel Odometry, Gauss-Newton, Optimal Control, Localization, Autonomous

Vehicle.

Abstract: In the motion estimation of self-driving vehicles, the three main requirements are accuracy, robustness, and

cost-effectiveness. The generally applied sensors and methods are the GNSS, inertial, and visual-odometry, but the contradictory requirements demand the integration of new ideas. The wheel odometry could be an adequate choice since the method is robust and cost-effective, but the accuracy of the estimation is limited by the parameter uncertainty, thus a calibration method should be included as well. However, the general parameter identification of a nonlinear model in the presence of noise has not been solved yet. The presented method is based on the assumption that noisy, but several measurements of GNSS and IMU sensors are available in a self-driving vehicle. In the proposed architecture, nonlinear least squares and optimal control techniques are combined in a unique way to compensate for the noise of the orientation and wheel rotation signals to achieve unbiased model calibration. The performance of the developed algorithm and the accuracy of parameter

estimation are demonstrated with detailed validation and a test with a real vehicle.

1 INTRODUCTION

State estimation plays a critical role in self-driving because trajectory planning and motion control are based on its results. The aim is to determine the velocities and pose signals as accurately as possible. Similarly, robustness and cost-efficiency are also important in the automotive industry, thus cost-effective automotive-grade types of sensors are applied generally. The disadvantages of the GNSS (Global Navigation Satellite System), IMU (inertial measurement unit), or vision-based methods can be mitigated with the integration of wheel encoder measurements (Funk et al., 2017), (Sebastian Thrun, 2006). An accurate wheel odometry model would open up new possibilities to eliminate the drawbacks of the usual global navigation-centered GNSS-inertial-visual estimation for vehicles (Gao et al., 2018), (Falco et al., 2017), for example, it would be possible to correct the pseudorange measurements of the GNSS modules, which improves the performance of the whole state estimation.

^a https://orcid.org/0009-0007-2157-4053

b https://orcid.org/0000-0003-3388-1724

Furthermore, in GNSS-denied environments, the necessity of wheel odometry is indisputable. However, the model suffers from parameter uncertainty. Therefore, this paper focuses on the calibration of the wheel odometry model, which is equivalent to the parameter identification of a nonlinear dynamic system. Generally, this type of optimization has not been solved yet, see e.g. (Schoukens and Ljung, 2019), and the problem is more difficult when the model calibration has to be performed with noisy signals.

The calibration problem of the wheel odometry model first appeared in the navigation task of small mobile robots and has also become a topic of investigation with the appearance of autonomous functions in the automotive industry. The related works operate with two different estimation methods. In the one, the parameter estimation is handled as a state filtering with the Augmented Kalman-filter (Martinelli and Siegwart, 2006; Brunker et al., 2017). The process assumes zero dynamics for the parameters, thus it is a simple way to identify unknown values, but the convergence and observability are questionable (Martinelli and Siegwart, 2006; Censi et al., 2013), and

a final stable value can not be obtained. The other method is to estimate the parameters as a regression problem, which, due to the nonlinear model, results in non-convex optimization. Its general solution is difficult, the methods such as (Censi et al., 2013; Seegmiller et al., 2013) manage the nonlinear problem with double linearization or separation, however these only operate with a simplified odometry model and almost perfect reference orientation measurements. In the case of a real-sized self-driving vehicle, these can not be presumed (Fazekas et al., 2020).

When parameters of a nonlinear model are identified, the key factor is the handling of the noise. Linear system identification is a well-explored area (Ljung, 1987), but due to nonlinearity, there are new issues that do not appear at all in the linear case. Since the dynamics from the inputs to the outputs is not linear, the impact of the input noise can not be modeled with Gaussian distribution (which assumption is applied in the methods such as Kalman-filtering or least squares) on the measured output (Schoukens and Ljung, 2019). Thus, the model calibration will certainly be biased, even in the case of white noise.

This distortion effect can be handled in two ways. The one is to apply specific requirements, such as unbiased estimation of the initial pose (Antonelli et al., 2005), measurement with expensive sensors (Lemmer et al., 2010), or special pre-defined measurement scenarios (Jung et al., 2016), etc. Only a few papers use the other way, which is to develop a unique algorithm that deals with the noise. In (Maye et al., 2016), an undesirable behavior of the traditional observability analysis is examined. The proposed algorithm detects the case when, due to the noise, the parameters seem to be observable, but in fact, they are not (e.g. the vehicle moves on a degenerate path for the calibration).

In parallel with the machine learning boom, studies apply machine learning techniques to the odometry calibration topic. In (Onyekpe et al., 2021), a neural network is trained to learn the pose error of a mobile robot, and an improved version in (He et al., 2023) for real-sized vehicles, but the online recalibration is not addressed. Other works, such as (Toledo et al., 2018) and (Zhang et al., 2021), approximate the whole odometry model instead of the error. Regardless of whether the error or the model is learned, special attention should be taken to avoid overfitting, as the training data's actual measurement error includes the noise and it is also approximated. Another disadvantage is that the industry prefers physical models to black-box models, especially for safety-critical systems such as automated road vehicles. Therefore, these can be rather a supplementary method and more important is the detailed physical modeling and the calibration of its parameters, before the approximation of the remaining error terms.

Our work addresses the direct compensation of the distortion effect of the noise. Any specific requirement is not applied, since a self-driving vehicle should recalibrate itself with the available onboard sensors. Only measurements of general driving in real streets are used, without any predefined path or input sequence. The main contribution is that the proposed calibration architecture includes noise compensation besides the traditional parameter identification. The algorithm operates with the Gauss-Newton nonlinear least squares method and an optimal control technique. The efficiency of the proposed algorithm is validated with experimental tests of a real-sized vehicle, which demonstrates that the mentioned issues of the noise are eliminated, and unbiased model calibration can be reached.

The remainder of the paper is organized as follows. In Section 2, the applied odometry model, including a dynamic wheel model, is presented. The general calibration method of a nonlinear model is described in Section 3. This section also outlines the problems and gives a brief review with motivation examples. The proposed improved calibration architecture with noise compensation can be found in Section 4. The validity of our approach is demonstrated via vehicle test experiments and detailed tests in Section 5, and finally, the paper is concluded in Section 6.

2 VEHICLE MODEL

The navigation with wheel odometry is based on a model, where the state vector x_t contains the pose, the longitudinal and lateral positions of the center of gravity $p_{x,t}$, $p_{y,t}$, and the ψ_t orientation of the vehicle, and change of the pose is based on the longitudinal v_{t-1} and angular ω_{t-1} velocities,

$$\begin{bmatrix} p_{x,t} \\ p_{y,t} \\ \psi_t \end{bmatrix} = \begin{bmatrix} p_{x,t-1} + v_{t-1} \cdot \cos(\psi_{t-1} + \frac{\omega_{t-1}}{2} + \beta_{t-1}) \\ p_{y,t-1} + v_{t-1} \cdot \sin(\psi_{t-1} + \frac{\omega_{t-1}}{2} + \beta_{t-1}) \\ \psi_{t-1} + \omega_{t-1} \end{bmatrix}.$$
(1)

The input u_t is composed of the $n_{l,t}$ effective wheel rotation signals (l = RL, RR rear-left/right), which are the slip free rotations, and the β_t sideslip angle of the vehicle.

The velocities are computed utilizing the wheel rotations,

$$v_t = (n_{RL,t} \cdot c_{RL,t} + n_{RR,t} \cdot c_{RR,t})/2,$$
 (2a)

$$\omega_t = (n_{RR,t} \cdot c_{RR,t} - n_{RL,t} \cdot c_{RL,t})/t_r, \qquad (2b)$$

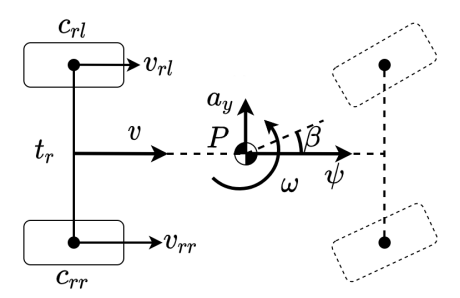


Figure 1: Odometry model.

where $c_{l,t}$ is the actual wheel circumference, and t_R is the rear track. The slight change of the wheel radius due to the effect of vertical dynamics is generally neglected, because the odometry-based localization is widely used in low-speed circumstances, e.g. automated parking. However, our method is developed for general driving, where the dynamics is significant, thus we apply the proposed model of (Fazekas et al., 2020), in which the change is considered, such as

$$c_{RL,t} = c_e + c_d/2 + d \cdot a_{v,t},$$
 (3a)

$$c_{RR,t} = c_e - c_d/2 - d \cdot a_{v,t},$$
 (3b)

where the c_e is the effective wheel circumference, c_d is the difference between the effective values, $a_{y,t}$ is the lateral acceleration, and the dynamic component d takes into account the effect of vertical dynamics. In the calibration process, every state variable is measured, thus the system model is

$$x_t = f(x_{t-1}, u_{t-1}, \theta), \quad x_t = [p_{x,t}, p_{y,t}, \psi_t]^T,$$
 (4a)

$$u_t = [n_{RL,t}, n_{RR,t}, \beta_t, a_{y,t}]^T, \quad y_t = x_t,$$
 (4b)

and the vehicle model parameters are arranged in the parameter vector,

$$\theta = [c_e, c_d, t_r, d]. \tag{5}$$

The values are illustrated in the paper with the units of m,mm,m,mm·s²/m for the c_e , c_d , t_r , d parameters, respectively. The nominal values of c_e and t_r can be found in the vehicle datasheet, but with these values, the position error of the model is already in the range of 10 m after a few hundred meters.

3 CALIBRATION OF NONLINEAR MODELS AND MOTIVATION EXAMPLES

3.1 Parameter Estimation with Gauss-Newton Method

Generally, the parameter estimation is formulated as a least squares (LS) optimization problem, to minimize

the error of the $\widehat{y}_k(\theta)$ predictor of the model from \widetilde{y}_k output measurements, such as

$$\widehat{\theta}_{opt} = \underset{\theta}{arg \ min} \ V_K(\theta) = \underset{\theta}{arg \ min} \ \sum_{k=1}^K ||\widetilde{y}_k - \widehat{y}_k(\theta)||^2,$$
(6)

When the model is nonlinear in θ the optimization can only be solved with numerical search (Tangirala, 2015). We apply the Gauss-Newton (G-N) method that solves the nonlinear least squares problem with Taylor-approximation in the following way,

$$\widehat{y}_{k}(\theta) \approx \widehat{y}_{k}(\theta_{i-1}) + \underbrace{\frac{\partial \widehat{y}_{k}(\theta)}{\partial \theta} \bigg|_{\theta_{i-1}}}_{j_{k}} \underbrace{(\theta - \theta_{i-1})}_{\Delta \theta}.$$
 (7)

Due to the dynamic behavior of the predictor, the j_k jacobians are computed recursively. This results in a locally linear LS problem, such as

$$\widehat{\Delta\theta}_{opt} = \underset{\Delta\theta}{arg \, min} \, \sum_{k=1}^{K} ||(\widetilde{y}_k - \widehat{y}_k(\widehat{\theta}_{i-1})) - j_k \Delta\theta||^2, (8)$$

which can be solved with the LS solution in an iterative way,

$$\widehat{\boldsymbol{\theta}}_i = \widehat{\boldsymbol{\theta}}_{i-1} + (J^T W J)^{-1} J^T W R, \tag{9}$$

where the $J := J(\widehat{\theta}_{i-1})$, $R := \widetilde{Y} - \widehat{Y}(\widehat{\theta}_{i-1})$ matrices are formed from the j_k and $(\widetilde{y}_k - \widehat{y}_k(\widehat{\theta}_{i-1}))$ values, respectively. A weight matrix W is also added to the basic solution. Since the model is linearized in the previous parameters, an initial guess for θ is required, and when in last term $(\widetilde{Y} - \widehat{Y}(\widehat{\theta}_{i-1}))$ the integrated system model is computed, the states have to be initialized at the beginning of the estimation window.

3.2 Problems of Nonlinear Parameter Estimation

The noise on the \widetilde{y}_t measured output would be less significant because it enters after the nonlinearity. However, when the R residual in (9) is formulated, the $\widetilde{y}_{t\to k=0}$ measured output has to be utilized for state initialization. Due to the appeared noise on it, the integrated model diverges from the correct path regardless of the vehicle parameters, which results in bias in the model calibration. Some paper tries to deal with the issue (Fazekas et al., 2021b), but the general solution is still an open question.

The noise on the u_t measured input must not be neglected, since its impact on the output can not be modeled with the Gaussian framework (Schoukens and Ljung, 2019). Because the methods like least squares or Kalman-filter apply this framework, the estimation would be biased. Therefore, our paper focuses on the compensation of both input and output noises to guarantee unbiased model calibration.

3.3 Motivation Examples of the Calibration and Compensation

Without calibration of the odometry model, c_d =0 and d=0, and nominal values as c_e =2 m, and t_r =1.55 m have to be utilized. The localization error with this setting is 6 m on 150 m long segments, thus the model without calibration is useless for vehicle localization.

The amount of distortion due to uncertain parameters and wheel rotation input noises, simulated signals are generated where the measured $(n_{RL/RR})$ wheel rotation signals are filtered with a Fourier-transformation, and these are utilized as inputs in the odometry model (4a) to form noise-free signals.

3.3.1 Impact of the Parameter Uncertainty and Initialization

The positioning uncertainty is almost linear with the parameter uncertainty. The circumference difference has the highest impact, the deviation of around 2 mm of c_d has the same 2 m mean position error as 2.5 cm of c_e , 5 cm of t_r , or 2 mm · s²/m of d parameter uncertainty.

The noisy measurements used for state initialization $(x_{k=0} = \widetilde{y_t})$ result in similar path divergence in the integrated model. For example, calibrating the model with additive Gaussian pose noises with $\sigma_{p_x} = \sigma_{p_y} = 0.2$ m, and $\sigma_{\psi} = 1.5^{\circ}$ standard deviation, the bias of the estimated parameters are 7.82e-04 m, 0.24 mm, 0.09 m, 1.26 mm for the c_e, c_d, t_r, d parameters, respectively. The consequence of these uncertain calibrations is a 2.26 m validation error on 150 m long routes. The noise on the orientation initialization is mainly responsible for the error, thus for proper odometry calibration, the measured orientation has to be corrected.

3.3.2 Impact of the Wheel Rotation Noise

For the examination of the impact of wheel rotation noise, generated Gaussian noise signals with $\sigma_{n,RL/RR} = 0.0005$ (at 50 km/h the $n_{RL/RR,t}$ signals are 0.17 due to the multiplication by the sampling time) are added to the filtered signals. Since the simulated pose signals are utilized for the calibration, the deviation from the noise-free case is induced only by the noise of the wheel rotation. The biases of the identified parameters are 0.0002 m, 0.31 mm, 0.25 m, 0.7 mm for the c_e, c_d, t_r, d parameters, respectively, but the middle 50% IQR ranges of the estimated values are spread within the 0.003 m, 1.2 mm, 0.1 m, 2.2 mm ranges. Previous examinations illustrate that these deviations result in significantly increased position error, which can be found in Figure 2. The 1 m

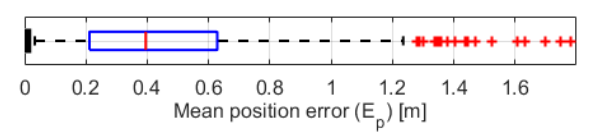


Figure 2: Mean position errors with $\sigma_{n,RL/RR} = 0.0005$ additive wheel rotation noise.

position error demonstrates the necessity of compensating the wheel rotation signals as well, since even with this generated noise with zero mean, the resulting localization inaccuracy is significant.

4 CALIBRATION METHOD WITH INTEGRATED NOISE COMPENSATION

4.1 Estimation in Batch Mode

The mentioned problems in Section 3.2 can be handled if more K long measurement segments are applied at once. In this batch mode, the matrices in the G-N method of the segments are concatenated into the following huge matrices (N denotes the batch size),

$$J_{B}(\widehat{\boldsymbol{\theta}}_{i-1}) = \begin{bmatrix} J_{1}(\widehat{\boldsymbol{\theta}}_{i-1}) \\ \vdots \\ J_{N}(\widehat{\boldsymbol{\theta}}_{i-1}) \end{bmatrix}, R_{B} = \begin{bmatrix} Y_{1} - \widehat{Y}_{1}(\widehat{\boldsymbol{\theta}}_{i-1}) \\ \vdots \\ Y_{N} - \widehat{Y}_{N}(\widehat{\boldsymbol{\theta}}_{i-1}) \end{bmatrix}.$$

$$(10)$$

The parameters can be identified in the same iterative way of (9) with the batch matrices, as

$$\widehat{\Theta}_{B,i} = \widehat{\Theta}_{B,i-1} + (J_B^T W_B J_B)^{-1} J_B^T W_B R_B, \tag{11}$$

In this case, the model fitting is performed on every segment simultaneously, which reduces the effect of noise. However, the distortion effect of the noises is only reduced but not eliminated, since the segment with the highest residual has a higher impact on the resulting common estimated parameters due to the minimization of the sum of residuals.

4.2 Input Compensation Method

The main inputs of the odometry model to be compensated are the effective wheel rotations, which will be noted as $u_{c,t} = [n_{RL,t}, n_{RR,t}]^T$. These are measured with the ABS encoder, but the quantities are corrupted by the slip and measurement noises.

For the compensation of the wheel rotation input noises, a minimization task is formed such as,

$$\min_{u_c(\cdot)} \sum_{k=1}^{K} L(\widetilde{y}_k, y_k(\theta), u_{c,k})$$
s.t.
$$x_k = f(x_{k-1}, u_{k-1}, \theta) \mid x_0 = \widetilde{y}_0$$
(12)

which is the general optimal control problem in discrete form $(y_k(\theta) = x_k$ the model output). The idea is motivated by the well-known model predictive control strategy, where the optimal input sequence can be determined with numerical optimization to satisfy the tracking of a future trajectory by the system.

In the nonlinear case, it is meaningful to apply quadratic cost functions and perform Jacobian linearization of the model around a nominal trajectory,

$$\widehat{A}_k = \frac{\partial f(\cdot)}{\partial x}\Big|_{\widehat{x}_k}, \qquad \widehat{B}_k = \frac{\partial f(\cdot)}{\partial u}\Big|_{\widetilde{u}_k}, \qquad (13a)$$

$$\widehat{g}_k = f(\widehat{x}_{k-1}, \widetilde{u}_{k-1}, \theta) - (A_k \widehat{x}_{k-1} + B_k \widetilde{u}_{k-1}).$$
 (13b)

With these considerations, the optimization problem (12) can be traced back to a locally linear predictive control minimization with equality constraints. The following task can be solved with quadratic programming (QP) techniques,

$$\min_{u_c(\cdot)} \sum_{k=1}^{K} ||\widetilde{y}_k - y_k(\theta)||_Q^2 + ||\Delta u_{c,k}||_R^2 \to \widecheck{u}_c(\cdot)$$
s.t.
$$x_k = \widehat{A}_k x_{k-1} + \widehat{B}_k u_{k-1} + \widehat{g}_k \mid x_0 = \widetilde{y}_0$$

s.t.
$$x_k = A_k x_{k-1} + B_k u_{k-1} + \widehat{g}_k \mid x_0 = \widetilde{y}_0$$

 $\underline{x}_k \le x_k \le \overline{x}_k, \ \underline{u}_{c,k} \le u_{c,k} \le \overline{u}_{c,k} \ k = 1...K$
(14)

where Q, and R are positive definite weighting matrices. The nominal trajectory $\widehat{x}_{k=1..K}$ is computed with the model (4a) utilizing the measured $\widetilde{u}_{c,k=1..K}$ wheel rotations. The QP solvers apply initial values for the optimization to which the measured values are applied as well.

4.3 Calibration Architecture

Our method operates with automotive-grade dual GNSS, IMU and wheel encoder sensors. The details of the measurements can be found in Section 5.1, now, assume to have measured pose $(\widetilde{p}_x, \widetilde{p}_y, \widetilde{\psi})$, wheel rotation $(\widetilde{n}_{RL}, \widetilde{n}_{RR})$, and the required additional inputs of the model (β, a_y) .

The aim of this paper is the proper model calibration through noise compensation. However, the optimal control task (12) supposes a known θ parameter, and correct pose values are required for the state initialization. Therefore, a complex architecture is proposed, which can be found in Figure 3. The algorithm operates with smaller segments divided from a long measurement, and it has the following 5 steps:

Step 1: Prior parameter estimation

To generate parameters for the input estimation, initial G-N identifications are performed in batch mode (Section 4.1) resulting $\widehat{\theta}_I$ values.

Step 2: Orientation correction

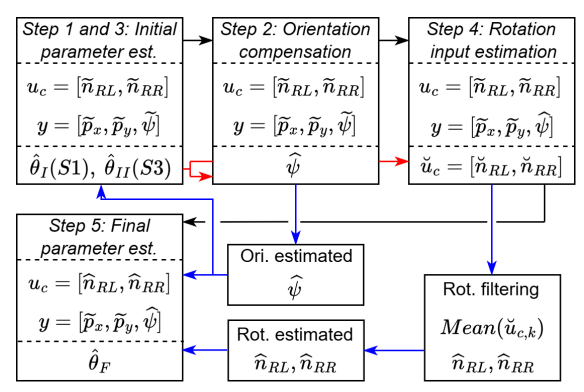


Figure 3: Architecture of the model calibration. In every step, the actual version of the utilized input and output signals are illustrated.

The wheel rotation compensation method presented in Section 4.2 is applicable for the orientation correction as well. As a result of the minimization, besides the optimal inputs, the states are also estimated. To minimize the trajectory error in (14), the evolution of estimated wheel rotation signals in the initial time instants generates a significant change in the orientation, which is equivalent to the compensation of the initialization error. The compensated orientation is formulated as,

$$\widehat{\Psi}_k = \widetilde{\Psi}_k + \Delta \Psi, \quad \Delta \Psi = (\widehat{\Psi}_{10}(\widehat{\theta}_I, \widecheck{u}_c) - \widetilde{\Psi}_{10}), \quad (15)$$

where $\widehat{\psi}_{10}(\theta_I, \widecheck{u}_c)$ is the orientation value with the estimated optimal inputs at the k=10 time moment. This compensation is performed for every segment of the batch individually.

Step 3: Compensated parameter estimation

Since the orientation signal of the segments is compensated, the same batch parameter estimation as in Step 1 is recalculated. In this way, $\widehat{\theta}_{II}$ initial parameters with increased accuracy are formulated for the input estimation.

Step 4: Rotation input estimation

The wheel rotation compensation is performed with the optimal control algorithm. The estimated $\widehat{\psi}_k$ values are utilized, and the vehicle model is parameterized with $\widehat{\theta}_{II}$. Since more $\widehat{\theta}_{II}$ values are available, the input estimation is performed more times, and compensated $\widehat{n}_{RL/RR}$ signals are formed as the mean of the middle 80% of \widecheck{u}_c estimations.

Step 5: Final parameter estimation

Finally, the vehicle parameters are identified in batch mode resulting in the $\widehat{\theta}_F$ identified values, but at this time in every segment, the compensated \widehat{n}_{RL} and \widehat{n}_{RR} inputs, and $\widehat{\psi}_k$ orientation are utilized.

4.4 Tuning of the Method Through an Illustration Example

In the Gauss-Newton parameter identification method, the W is introduced to equalize the lower value of orientation error in radians, than the position errors in meters. The experimental tuning results in the following setting

$$w = [w_{p_x}, w_{p_y}, w_{\Psi}] = [1, 1, 50], \quad W = [w, ..., w]_{1 \times 3K}$$

to obtain proper vehicle model calibration. Due to the linearization in the G-N method, an initial guess for the parameters is necessary, for which the nominal values as $\theta_{nom} = [2,0,1.55,0]$ from the vehicle's datasheet are applied. The maximum iteration of the G-N method is 5.

Since in our optimal control problem the estimated inputs are measured and close to the effective ones, a relatively high prediction horizon K = 650 can be applied. For maximum iteration, 10 is sufficient, due to the limits being chosen such as,

$$\underline{x}_k = \widetilde{y}_k - [5, 5, 0.5], \quad \overline{x}_k = \widetilde{y}_k + [5, 5, 0.5],$$

 $\underline{u}_{c,k} = \widetilde{u}_{c,k} \cdot 0.95, \quad \overline{u}_{c,k} = \widetilde{u}_{c,k} \cdot 1.05.$

The main tuning parameters of the optimal control task are the Q and R weighting matrices as $Q = diag([q_{p_x}, q_{p_y}, q_{\psi}])$ and $R = diag([r_{n_{RL}}, r_{n_{RR}}])$. Ensuring the trajectory tracking without high-frequency changes of inputs, the weights are chosen, such as

$$q_{p_x} = 1$$
, $q_{p_y} = 1$, $r_{n_{RL}} = 1000$, $r_{n_{RR}} = 1000$, $q_{\Psi} = 1$ in Step 2, $q_{\Psi} = 10$ in Step 4.

The batch size of the G-N method and the number of input estimations to form the compensated signals influence the accuracy of model calibration. The batch size is fixed through the algorithm to N=9, and when the $\widehat{n}_{RL/RR}$ signals are estimated, 12 input estimations are performed.

5 RESULTS

5.1 Test Vehicle and Measurement

The test vehicle is equipped with automotive-grade GNSS, compass, and IMU sensors, and from the vehicle's CAN bus, the wheel encoder signals are also saved with 0.025 s sampling time. The test track is a 24 km long route in suburban and city driving, containing various bends, two roundabouts, and lots of crossroads.

The signals of the GNSS, compass, and IMU sensor are utilized in a Kalman-filter (Caron et al., 2006)

to compute the measured \widetilde{p}_x , \widetilde{p}_y , $\widetilde{\psi}$ pose values. The sideslip is also estimated with an IMU-based method (Fazekas et al., 2021a) in the bends.

The calibration architecture operates with smaller measurement parts, therefore, the route is divided into segments with 150 m average length. Since the c_d , t_R and d parameters can be appropriately observed only with the yaw rate equations (2b), the 896 segments with absolute angular velocity higher than $0.15 \ rad/s$ are selected for the parameter estimation. Using these segments, 1000 various batches are formulated.

5.2 Validation Process and Error

The true value of the $\theta = [c_e, c_d, t_R, d]$ parameters are unknown, thus the presented method is validated with the position error of the calibrated models. In order to avoid overfitting, the segments are regenerated with 300 m average length for the validation. The position error of a calibration containing $\hat{\theta}$ is calculated for every segment s,

$$E_{p,s} = \sum_{k=1}^{K} \sqrt{(\widetilde{p}_{x,k} - p_{x,k}(\widehat{\boldsymbol{\theta}}))^2 + (\widetilde{p}_{y,k} - p_{y,k}(\widehat{\boldsymbol{\theta}}))^2}$$
(16)

and the $E_p = \overline{E_{p.s}}$ average of these is applied as a validation error to evaluate the calibration.

The minimum validation error is not zero, because the states of the odometry model (4a) at the beginning are initialized with the \tilde{y}_t measured pose values, and raw $\tilde{n}_{RL/RR,t}$ rotations are utilized. The reachable limit in this validation case is 2.42 m, and the calibrations are presented compared to this value.

5.3 Prior Model Calibrations

To reach initial estimated parameters, the batch G-N method (Section 4.1) is utilized on the formulated 1000 batches. In Step 1, the raw measured \tilde{y}_t pose and $\tilde{n}_{RL/RR,t}$ rotations are utilized. The estimated parameters can be found in Figure 5, the standard deviations of the quantities are high, e.g. the track width reaches both 1.45 m and 1.65 m, which are unrealistic. The top boxplot of Figure 6 shows the validation error, the median value is 0.8 m, but due to the uncertain parameters, the error reaches 3.5 m.

5.4 Orientation Compensation and Illustration of the Input Estimation

It has been mentioned that an interesting property of the input estimation is the capability of correcting the orientation measurement uncertainty as well. For a

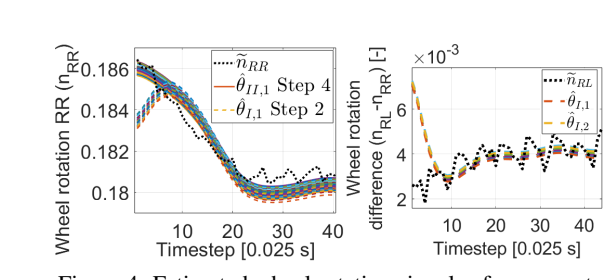


Figure 4: Estimated wheel rotation signals of a segment.

segment, the orientation correction (Step 2) is performed with more θ_I prior parameters. The left of Figure 4 presents a part of the estimated wheel rotations. The estimated signals are close to each other with a similar shape. In the case of orientation correction, the difference of the rotations is worth examining in the right of Figure 4.

Initially, the difference between the estimated signals is significantly greater than the difference between the measured rotations, indicating a deterministic occurrence. The change of the wheel rotation difference induces additional angular velocity, thus the orientation can be compensated via the input estimation method.

The estimated orientation difference $(\Delta \psi)$ of all of the segments in the batches is in the range of $\pm 3^{\circ}$ with IQR of [-0.7°,0.6°], which has a significant impact on the estimations, therefore the orientation compensation is absolutely necessary.

In Step 4, the same input estimation is executed with the segments as in Step 2, but the $\widehat{\psi}$ estimated orientation is utilized. The left of Figure 4 shows that the fall at the beginning disappeared owing to the improved initialization, and the estimated rotations are around the measured ones. However, the plot illustrates that the optimized trajectory tracking induces smoother wheel rotations and verifies the assumption of noisy measured signals. The variety of the estimations is filtered out with the formulation of the mean of the \widecheck{u}_c signals to reach $\widehat{n}_{RL/RR}$.

5.5 Calibration with the Proposed Method and Validation

Finally, in Step 5, the vehicle parameters are estimated in batch mode utilizing the estimated $\widetilde{\psi}$ and $\widetilde{n}_{RL/RR}$ signals. For comparison, the same batches are used as in Step 1. The process illustrated in Figure 3 is performed for every batch. The estimated parameters of the 1000 batches are shown with box-plots in Figure 5. The medians of the identified parameters are almost the same as in Step 1 with the pure batch G-N, but the standard deviations of the calibrations decrease substantially.

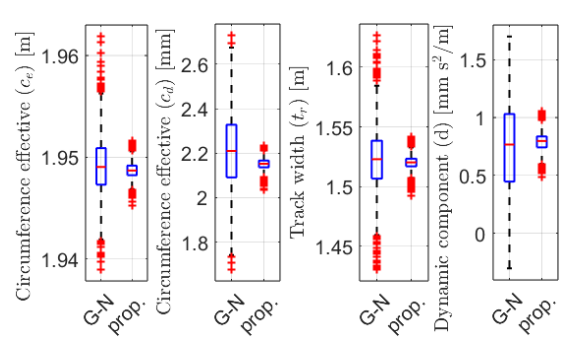


Figure 5: Box-plots of the estimated parameters with the pure (Step 1) and proposed (Step 5.) method.

The ranges of the middle 50% of the parameters are decreased by 78%, 87%, 80% and 84%, of the c_e , c_d , t_r , d parameters, while the spreads of estimations are approximately the same by 75% on average, respectively.

The validation errors of the calibrated models in Step 1 and 5 can be found in Figure 6 with box-plots. This demonstrates the significant improvement with the proposed algorithm, and the impact of the noise on the measured signals as well.

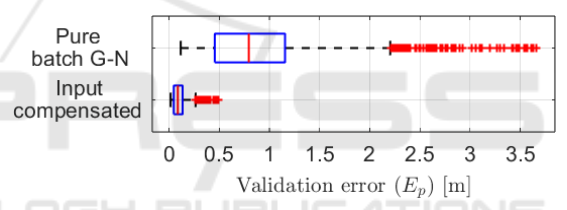


Figure 6: Box-plots of the validation errors with the pure batch G-N technique in Step 1, and the final estimation with the compensations in Step 5.

When the compensated $\widehat{n}_{RL/RR}$ rotations are utilized, the calibration accuracy is increased on average, and furthermore, the calibrations with higher errors disappear. These should be the cases when the distortion is induced by the input noise. Compared to the baseline pure batch G-N calibrations, using the proposed method, the worst model with the compensated signals has a lower error than the 25th percentile with the uncompensated signals. Considering the reachable limit, the median validation error is only 0.1 m, which indicates a nearly bias-free model calibration owing to the compensation of the noisy signals with the highest influence.

6 EVALUATION AND CONCLUSION

In this paper, a novel architecture integrating the compensation of the wheel rotation input noises was presented for the calibration of the nonlinear odometry model of a vehicle. This is performed with the batch version of the Gauss-Newton algorithm for the parameter estimation, and with the MPC-type optimal control technique for the input compensation. The main contribution of the paper is that, before the parameter identification, wheel rotation noises are compensated in an optimal way to reach the bias-free model calibration. In the future, we would like to examine this input estimation from a theoretical context and expand the method as a general parameter identification tool for the calibration of nonlinear models.

ACKNOWLEDGEMENTS

The work of Mate Fazekas has been implemented within the project no. MEC-R-24 with the support provided by the Ministry of Culture and Innovation of Hungary from the National Research, Development and Innovation Fund, financed under the MEC-R 149345 funding scheme. The research was supported by the European Union within the framework of the National Laboratory for Autonomous Systems (RRF-2.3.1-21-2022-00002).

REFERENCES

- Antonelli, G., Chiaverini, S., and Fusco, G. (2005). A calibration method for odometry of mobile robots based on the least-squares technique: theory and experimental validation. *IEEE Transactions on Robotics*, 21(5):994–1004.
- Brunker, A., Wohlgemuth, T., Frey, M., and Gauterin, F. (2017). GNSS-shortages-resistant and self-adaptive rear axle kinematic parameter estimator (SA-RAKPE). In 28th IEEE Intelligent Vehicles Symposium.
- Caron, F., Duflos, E., Pomorski, D., and Vanheeghe, P. (2006). GPS/IMU data fusion using multisensor Kalman-filtering: Introduction of contextual aspects. *Information Fusion*, 7(2):221–230.
- Censi, A., Franchi, A., Marchionni, L., and Oriolo, G. (2013). Simultaneous calibration of odometry and sensor parameters for mobile robots. *IEEE Transactions on Robotics*, 29(2):475–492.
- Falco, G., Pini, M., and Marucco, G. (2017). Loose and tight gnss/ins integrations: Comparison of performance assessed in real urban scenarios. Sensors, 17(2).
- Fazekas, M., Gáspár, P., and Németh, B. (2021a). Calibration and improvement of an odometry model with dynamic wheel and lateral dynamics integration. Sensors, 21(2).
- Fazekas, M., Gáspár, P., and Németh, B. (2021b). Estimation of wheel odometry model parameters with im-

- proved gauss-newton method. In *IEEE International Conference on Multisensor Fusion and Integration*.
- Fazekas, M., Németh, B., Gáspár, P., and Sename, O. (2020). Vehicle odometry model identification considering dynamic load transfers. In 28th Mediterranean Conference on Control and Automation, pages 19–24.
- Funk, N., Alatur, N., and Deuber, R. (2017). Autonomous electric race car design. In *International Electric Vehicle Symposium*.
- Gao, Z., Ge, M., Li, Y., Chen, Q., Zhang, Q., Niu, X., Zhang, H., Shen, W., and Schuh, H. (2018). Odometer, low-cost inertial sensors, and four-gnss data to enhance ppp and attitude determination. *GPS Solutions*, 22(57):147–159.
- He, K., Ding, H., Xu, N., and Guo, K. (2023). Wheel odometry with deep learning-based error prediction model for vehicle localization. *Applied Sciences*, 13(9).
- Jung, D., Seong, J., bae Moon, C., Jin, J., and Chung, W. (2016). Accurate calibration of systematic errors for car-like mobile robots using experimental orientation errors. *International Journal of Precision Engineering* and Manufacturing, 17(9):1113–1119.
- Lemmer, L., Heb, R., Krauss, M., and Schilling, K. (2010). Calibration of a car-like mobile robot with a high-precision positioning system. In 2nd IFAC Symposium on Telematics Applications.
- Ljung, L. (1987). System Identification: Theory for the User. PTR Prentice Hall.
- Martinelli, A. and Siegwart, R. (2006). Observability properties and optimal trajectories for on-line odometry self-calibration. In *IEEE Conference on Decision and Control*, pages 3065–3070.
- Maye, J., Sommer, H., Agamennoni, G., Siegwart, R., and Furgale, P. (2016). Online self-calibration for robotic systems. *The International Journal of Robotics Research*, 35(4):357–380.
- Onyekpe, U., Palade, V., Herath, A., Kanarachos, S., and Fitzpatrick, M. E. (2021). Whonet: Wheel odometry neural network for vehicular localisation in gnss-deprived environments. *Engineering Applications of Artificial Intelligence*, 105:104421.
- Schoukens, J. and Ljung, L. (2019). Nonlinear system identification: A user-oriented roadmap. *IEEE Control Systems Magazine*, 39(6):28–99.
- Sebastian Thrun, e. a. (2006). Stanley: The robot that won the DARPA Grand Challenge. *Journal of Field Robotics*, 23(9).
- Seegmiller, N., Rogers-Marcovitz, F., Miller, G., and Kelly, A. (2013). Vehicle model identification by integrated prediction error minimization. *The International Journal of Robotics Research*, 32(8).
- Tangirala, A. K. (2015). Principles of System Identification: Theory and Practice. CRC.
- Toledo, J., Piñeiro, J. D., Arnay, R., Acosta, D., and Acosta, L. (2018). Improving odometric accuracy for an autonomous electric cart. Sensors, 18(1):200–2015.
- Zhang, Z., Zhao, J., Huang, C., and Li, L. (2021). Learning end-to-end inertial-wheel odometry for vehicle egomotion estimation. In 5th CAA International Conference on Vehicular Control and Intelligence.